

# Turbidity-adaptive underwater image enhancement method using image fusion

Bin HAN<sup>a</sup>, Hao WANG<sup>a</sup>, Xin LUO (✉)<sup>a</sup>, Chengyuan LIANG<sup>a</sup>, Xin YANG<sup>b</sup>, Shuang LIU<sup>a</sup>, Yicheng LIN<sup>a</sup>

<sup>a</sup> School of Mechanical Science and Engineering, Huazhong University of Science and Technology, Wuhan 430074, China

<sup>b</sup> Guangdong Intelligent Robotics Institute, Dongguan 523808, China

✉ Corresponding author. E-mail: mexinluo@hust.edu.cn (Xin LUO)

© Higher Education Press 2022

**ABSTRACT** Clear, correct imaging is a prerequisite for underwater operations. In real freshwater environment including rivers and lakes, the water bodies are usually turbid and dynamic, which brings extra troubles to quality of imaging due to color deviation and suspended particulate. Most of the existing underwater imaging methods focus on relatively clear underwater environment, it is uncertain that if those methods can work well in turbid and dynamic underwater environments. In this paper, we propose a turbidity-adaptive underwater image enhancement method. To deal with attenuation and scattering of varying degree, the turbidity is detected by the histogram of images. Based on the detection result, different image enhancement strategies are designed to deal with the problem of color deviation and blurring. The proposed method is verified by an underwater image dataset captured in real underwater environment. The result is evaluated by image metrics including structure similarity index measure, underwater color image quality evaluation metric, and speeded-up robust features. Test results exhibit that the method can correct the color deviation and improve the quality of underwater images.

**KEYWORDS** turbidity, underwater image enhancement, image fusion, underwater robots, visibility

## 1 Introduction

Clear, correct imaging is a prerequisite for underwater operations, for example, localization of fish [1], control of underwater vehicles [2], rescue and salvage of sunken vessel, and antiterrorism action [3]. Especially, when observing or tracking fish at the bottom of the lake or sea, the fish can run away and raise the soil and sand at the bottom of the lake or sea, which will make that part of the water more turbid than others. In this situation, turbidity is variable, and using enhancement methods focusing on a single environment to solve it is not reasonable. However, problems of this situation will be solved if turbidity can be detected and the corresponding methods are selected, which is meaningful for underwater robotics. Thus, the turbidity-adaptive enhancement method, which can detect turbidity and use proper methods to process underwater images, is proposed in this paper.

Many studies about underwater imaging enhancement have been conducted. For example, combining optics with image processing technology, a novel image

dehazing method was devised and mainly used to solve the problems caused by backscattering in turbid water [4]. A Bayesian retinex algorithm for enhancing single underwater image with multi-order gradient priors of reflectance and illumination was developed [5]. The underwater image enhancement benchmark dataset (UIEBD) was used to verify the method. Liang et al. [6] proposed a systematic underwater image enhancement method, which included an attenuation map guide underwater image color correction approach and a detail preserved dehazing approach. Images used for test algorithm were captured from a real-world marine environment. An underwater image enhancement network via medium transmission-guided multicolor space embedding was presented in Ref. [7]. In the paper, many datasets were used, and many enhancement methods were compared. References [8,9] proposed an underwater enhancement method based on image fusion. Although these enhancement methods could improve the quality of underwater images, they did not consider the variation of the real-world environment, which means the water they worked on was single and static. For other environments, such as a moderate turbid underwater or an environment

varying with time or area, these methods could not be guaranteed to work as well as in their environments, which is the first problem found in this work.

In the real world, the characteristics of water, including turbidity, color, and the turbid medium, vary in different areas and time. The problems of images are also different. For example, the image of the sea environment studied in Ref. [8] usually suffers from color deviation, and the influence of scattering exists though small. However, for several turbid underwater environments, such as the Yangtze River and the Yellow River of China, the water is quite turbid because of large amounts of soil and sand. Compared with scattering, the influence of absorption is very small. Moreover, even in the same area water environment, the environment can vary with season or weather. The single enhancement method cannot be ensured to work well always. For a complex underwater environment, artificial intelligence (AI) is generally used for image enhancement [10,11]. Liu et al. [12] set up an undersea image capturing system and constructed a large-scale real-world underwater image enhancement, which could clearly improve image quality. Fu and Cao [13] proposed a two-branch network to compensate for the global distorted color and local reduced contrast, and designed a compressed-histogram equalization to complement data-driven deep learning. They used two ground truth datasets for their experiments, underwater color cast set and 200 real images from the Internet. These methods have a good effect on underwater image enhancement, but whether these AI methods can work well in severe turbid underwater environment is uncertain, which is the second problem proposed. Moreover, the effect of AI methods depends on the richness of data sets. To obtain good image enhancement methods based on AI, rich image sets are essential. However, underwater image sets are insufficient for special environments, such as severe turbid water or polluted water with artificial factor. Now many researchers are solving the problem. Yang et al. [14] addressed the problem based on a conditional generative adversarial network. They used synthesized underwater images and two underwater image sets to test their algorithm. Jiang et al. [15] presented a two-step domain adaption enhancement method that does not require training on synthetic underwater images and eliminates the dependence on underwater ground-truth images. Li et al. [16] constructed a UIEBD including real-world underwater images and corresponding reference images. However, relevant datasets for severe turbid underwater are rare. Hence, a traditional underwater enhancement method that can adapt to different environments and address the limitation of the underwater dataset is essential.

The adaptive method in this paper is based on the proposed turbidity method, which can classify different underwater environments. Many studies on turbidity detection have been conducted. In Ref. [17], turbidity

detection methods were divided into four areas, namely, sample images, underwater images, water surface images, and invisible light images. To enhance underwater images, the research of turbidity detection focuses on the area of the underwater image. In this area, different effective, reasonable detection methods [18–20] were proposed, but they rely on datasets or have difficulty mapping the results to different underwater environments. Most of them focus on theory of expression of underwater turbidity. In addition, they can only detect turbidity without color deviation or deviation channel. Our turbidity detection method based on histograms is proposed to classify different environments, which can obtain the turbidity level, color deviation level, and deviation channel. The work by Ref. [21] is relatively similar to ours. In Ref. [21], the author recognized different environments based on convolution network and enhancement images based on dark channel prior (DCP). Different environments were classified, but the enhancement methods were all same, and the only difference was the value of the variables of post processing. Adjusting values is not sufficient for environments with great differences. Thus, a decision making method to detect image turbidity, which is important for our image enhancement method, is proposed.

The second problem for most general studies is the disregard for moderate harsh underwater environment. This paper notes two features for the moderate harsh underwater environment. First, it is so turbid that the main object is difficult to identify. Second, it has an unnatural color deviation. Underwater image enhancement [4–7,9–14] and turbid underwater [20–23] work well in the environments of their papers, but their images are not very turbid even though several of them focus on turbid environments. Image enhancement for several very turbid environments, such as the Yangtze River or polluted waters, is essential. Moreover, papers about underwater image enhancement believe that the most serious attenuation channel of underwater is red, consequently, the underwater image is dominated by blue or green [24]. This theory is correct in common water, such as sea or clean rivers. However, this condition changes if colored things are in the water, such as dyestuff or polluted items. In this paper, many partially red underwater images, which are impossible in the common underwater environment, are captured. Considering harsh environments, concluding that underwater images are dominated by blue or green is not proper. The colored things in water and the artificial factor should also be considered. To deal with the problem, turbidity detection is combined with a new image enhancement method, which can correct color based on the real color deviation. Experiments are carried out to capture turbid underwater images that meet the requirement of severe turbidity level in this paper. The proposed method solves the two above problems.

## 2 Underwater imaging model

Ignoring forward scattering, the imaging model based on Jaffe [25] can be obtained as follows:

$$I^c(x) = J^c(x)T^c(x) + (1 - T^c(x))B_\infty(x)^c, \quad c \in \{R, G, B\}, \quad (1)$$

where  $I^c(x)$  is the pixel value at  $x$  of color channel  $c$  of degraded image,  $x$  is the localization of pixel,  $c$  denotes the color channel,  $B_\infty(x)^c$  is the value of infinite pixel  $x$  of color channel  $c$  of ambient light image, and  $J^c(x)$  is the pixel value at  $x$  of color channel  $c$  of original image.  $T^c(x)$ , which is the pixel value at  $x$  of color channel  $c$  of transmission map, can be written as follows:

$$T^c(x) = \exp(-\alpha d(x)), \quad (2)$$

where  $\alpha$  is the attenuation coefficient of water, and  $d(x)$  is the object distance of pixel  $x$ .  $\alpha$  is close to 0 in clear water [26] and higher in severe turbid water. For turbid underwater environments, serious scattering is caused by particles, which makes the underwater images, especially with artificial lighting, covered with haze. In clear water, the main problem becomes the color deviation caused by the absorption of water. Several images captured in our experiments are selected to explain the situation in Fig. 1. For the image of light turbidity, color deviation is observed, and the color is slightly green. With the growth of turbidity level, color deviation becomes smaller, and the influence of scattering worsens. For the image of severe turbidity, color deviation can be ignored, but blur prevents identifying the object in the image. Depth influences the color deviation of underwater images, but the influence is more apparent in clear water. In turbid water, the main influence is caused by scattering.

Based on the differences of turbid underwater environments, targets for each turbidity level are set, and an adaptive method composed of a series of methods is proposed.

In relatively clear underwater environments, to obtain a result with the correct color and rich details is reasonable, but it will be not practical in severe turbid environments because of high noise and blurry image. For images captured in these severe turbid environments, identifying the main object is more important than obtaining rich details. Thus, dissimilar targets are set for different environments. For light or medium turbid environments, the desired image has the correct color and rich details, whereas for severe turbid environments, the main object should be identified, and the color should be correct.

Turbidity detection is essential for underwater image enhancement, especially for turbid environments. Different enhancement methods should be used for various turbid environments and problems.

## 3 Proposed method

### 3.1 Turbidity detection

Considering many existing turbidity detection methods, our detection method is proposed based on histogram images, which can rapidly detect turbidity, the channel of color deviation, and the color deviation level of underwater images.

First, histograms of more than 300 different underwater images, several of which often appear in underwater image enhancement papers, and others are captured from our experiments, are researched. Then, two features in the histograms of these underwater images are found.

First, the channels of turbid underwater images are narrower than clear images, as shown in Fig. 2. The shape of the channel of clear underwater images is wide and uniform but it is narrow and high in turbid underwater images. Second, the deviation channel conforms to the deviation color.

If the underwater image is reddish, such as the red image of the color deviation underwater image in Fig. 2, the value of the red channel is higher than that of the other channels. The two features are the bases for our turbidity detection.

The first feature describes the turbidity level, and the second feature describes the color deviation channel and deviation level.

For the first feature, the variance of channels  $I_{\text{var}}$  denotes the turbidity level because it can represent the differences in histogram shapes. Two thresholds based on our images are set, and the turbidity levels are classified:

$$\text{Turbidity}_{\text{level}} = \begin{cases} \text{Severe,} & I_{\text{var}} < T_1, \\ \text{Medium,} & T_1 \leq I_{\text{var}} \leq T_2, \\ \text{Light,} & T_2 < I_{\text{var}}, \end{cases} \quad (3)$$

where  $T_1$  and  $T_2$  are the variance thresholds for turbidity level detecting, and they are set as 9 and 28 based on our tests, respectively.

For the second feature, the means of channels and the difference of the maximum and minimum means are

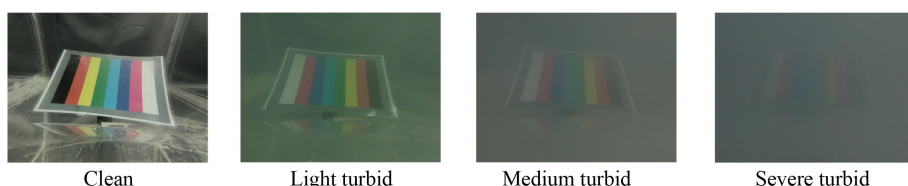


**Fig. 1** Images of standard color plate in different underwater environments.

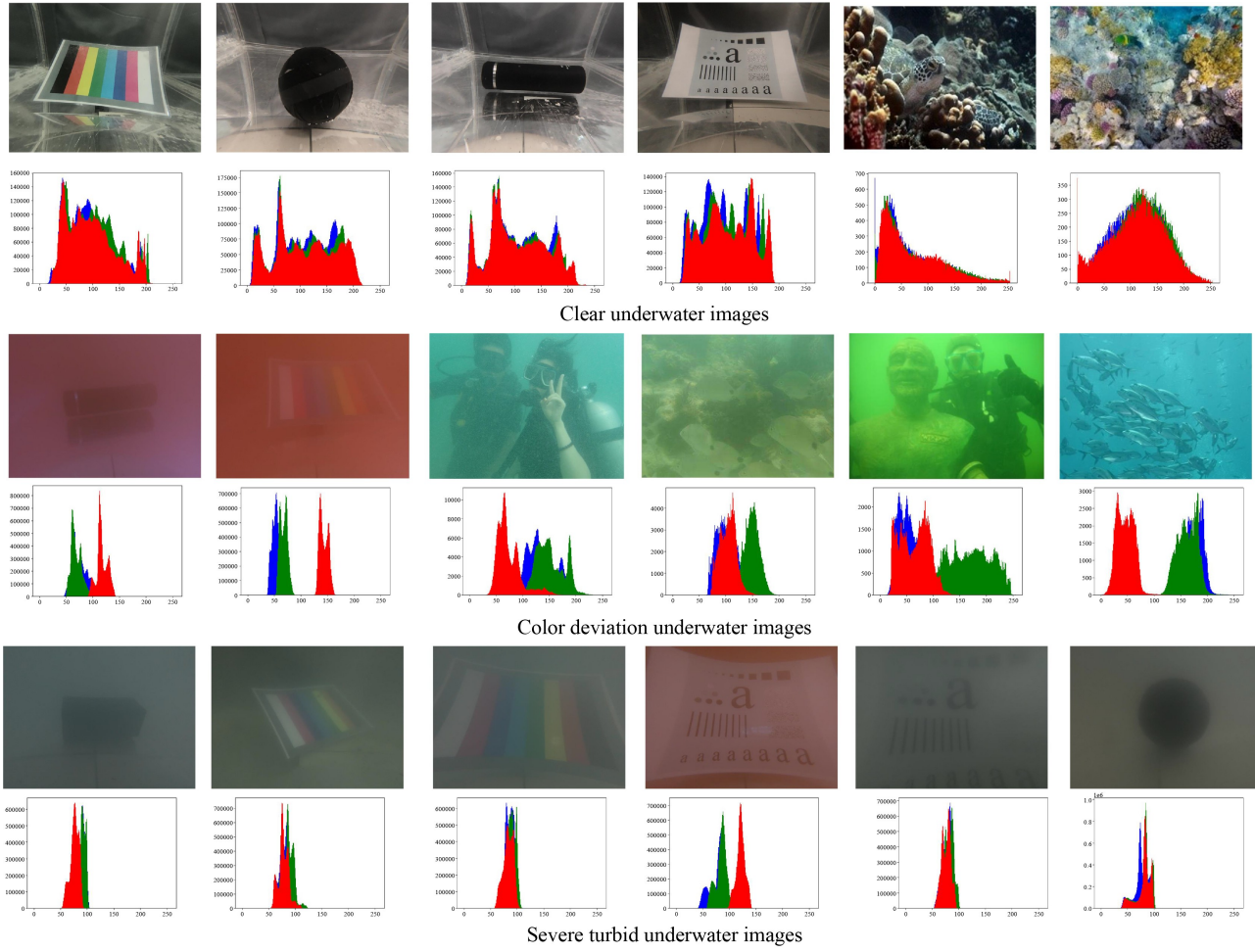


**Fig. 2** Histogram of underwater images with different turbidity.

adopted to describe the color deviation and color deviation level. The means of every single channel are calculated first, and then deviation is derived by subtracting  $Mean_c$  and  $Mean_{sum}$ :

$$\begin{cases} Mean_{sum} = \frac{1}{3} \sum_{c \in \{R, G, B\}} Mean_c, \\ Deviation_c = Mean_c - Mean_{sum}. \end{cases} \quad (4)$$

To correct the color deviation of underwater images, channel compensation is usually applied, which needs to know the attenuation channel. The attenuation channel is obtained in this section for our channel compensation method. The minimum of the three channels is selected as the attenuation channel. In the above images and histograms, the deviation channel is farther from other channels if the color deviation is severe. Hence, the difference of maximum and minimum  $Mean_c$  expresses the color deviation level:

$$Deviation_{max} = \max(Mean_c) - \min(Mean_c),$$

$$Deviation_{level} = \begin{cases} \text{Light,} & Deviation_{max} < L_1, \\ \text{Medium,} & L_1 \leq Deviation_{max} \leq L_2, \\ \text{Severe,} & L_2 < Deviation_{max}, \end{cases} \quad (5)$$

where  $L_1$  and  $L_2$  are the thresholds for color deviation level detecting, and they are set as 40 and 60, respectively.

Parts of our detection results are shown in Fig. 3. In this paper, the requirement for severe turbid is strict, consequently, images of most research about underwater image or turbid underwater image enhancement [26–28] cannot meet the requirement. They are classified as light turbid or medium turbid because they are not very turbid. Most severe turbid images are captured in our experiments.

### 3.2 Equalization gray world method based on channel compensation for color correction

Improvement of color and contrast is important for images [27,29]. Many studies [30–32] on underwater image color correction have been conducted, and they all work well in their environments. However, for several situations in this paper, such as turbid water with colored things, these methods cannot work as well as in their environments. In addition, many methods [9,24,33] are based on the theory that underwater images are

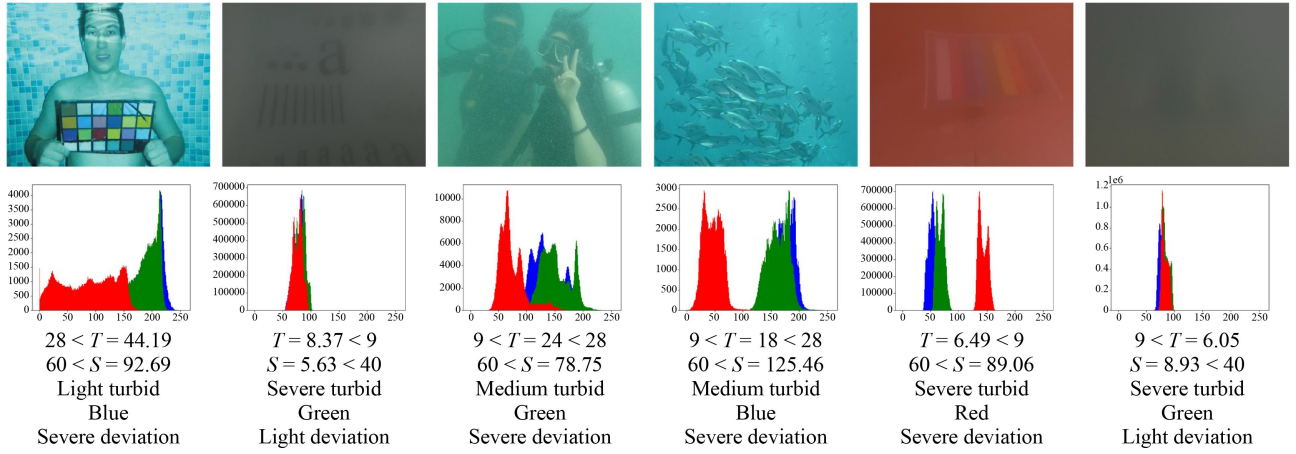


Fig. 3 Turbidity detection results of different underwater images.

dominated by blue or green, which is correct in common environments but does not apply to the situation in this paper. To deal with the problem, the equalization gray world method is proposed. In this method, the attenuation channel is first compensated based on the detection results. Then, histogram equalization is combined with the gray world, which works well in most images, but the results on underwater images still have color deviation. Moreover, because histogram equalization can also correct the color cast of underwater images with the result having a slight distortion, the two methods are combined, and the result is better than that of the single methods.

The three channels of images are assumed not independent. The two other channels and the attenuation channel are complementary in color information, and the two other channels are important for attenuation channel compensation. Thus, channel compensation is adopted in this section. The attenuation channel is compensated by the two other channels, and the compensation level is related to the deviation level. The severer attenuation of the channel is, the higher compensation level. A restriction is added because the color information in the attenuation channel is distorted if the compensation level is very high.

Compensation channel  $C_{jc}$  can be derived as follows:

$$C_{jc}(x) = \frac{C_{i1}(x) + C_{i2}(x)}{2} \left( \frac{\overline{C}_{i1} + \overline{C}_{i2}}{2\overline{C}_j} - 1 \right) w, \quad (6)$$

where  $\overline{C}_j$  is the mean of attenuation channel,  $C_{i1}$  and  $C_{i2}$  are two other channels.  $i$  and  $j$  are dependent on the attenuation channel of the image.  $\overline{C}_{i1}$  and  $\overline{C}_{i2}$  means the average of  $C_{i1}$  and  $C_{i2}$ .  $w$  is the parameter of compensation level, which is related to the color deviation level of the image and written as follows:

$$w = m + n \cdot Deviation_{level}, \quad (7)$$

where  $m$  and  $n$  are constant parameters for compensation.

In practice, our tests reveal that  $m = 0.18$  and  $n = 0.15$  are appropriate for different underwater images. The

results of channel compensation are shown in Fig. 4, where the attenuation channel of histograms after compensation is closer to that of the other channels. Based on the channel compensation, the images are further processed with our white balance method combining histogram equalization with gray world. Histogram equalization adjusts the histogram of images and improves the contrast of images. However, as mentioned above, histogram equalization can also adjust the color of images, although the results have a slight distortion. The luminance of images of histogram equalization is very high, which leads to difficulty in identifying images. For white balance, the gray world can work well in correcting color deviation, but the result is still red for several underwater images.

Considering the above problems, the two methods based on channel compensation are combined. The result of histogram equalization and gray world is obtained independently, and then the two images are fused with the proper weight adjusted by the result of turbidity detection. Through the white balance method, the color of images is improved, and the transmission maps are better than the original images. The results of our method are shown in Fig. 5, and the transmission maps are shown in Fig. 6.

### 3.3 Dehazing based on DCP

There are many dehazing methods [34–36], and their effect is good in improving image quality. However, they are usually combined with other functions such as color correction or contrast improvement, and they are not suitable to be combined into the whole enhancement frame of this paper. Thus, our dehazing method by improving DCP and combining it with the fast guide filter is proposed.

The model of our DCP method is the same as Eqs. (1) and (2). Reference [34] found that at least one channel has a low intensity, which can be written as follows:

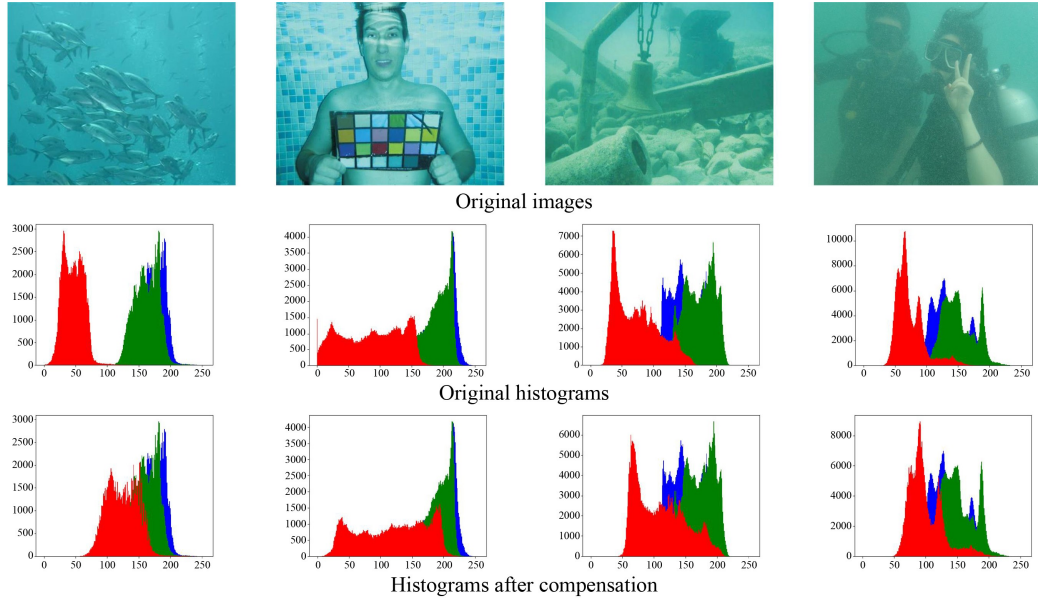


**Fig. 4** Comparative results of histograms before and after white balance.



**Fig. 5** Comparison of histogram equalization, gray world, and our method.

$$J_{\text{dark}}(x) = \min_{y \in \Omega(x)} \min_{c \in \{\text{R,G,B}\}} J^c(y) \approx 0, \quad (8)$$

where  $J_{\text{dark}}$  means the dark channel images,  $\Omega(x)$  denotes the local region centered at pixel  $x$ , and  $y$  is the pixel of region  $\Omega(x)$ .

The input of DCP in this paper is the result of white balance. To improve the transmission map of underwater images, the guide filter is improved [37]. According to Ref. [37], the great ratio of guide filter has a better effect for most processing. Based on our test shown in Fig. A1 in the Appendix, the ratio of filter is set as 50. The transmission map  $T(x)$  can be derived as follows:

$$\eta = 0.5 + 0.15 \text{Turbidity}_{\text{level}}(I_k), \quad (9)$$

$$T(x) = 1 - \eta \min_{y \in \Omega(x)} \left[ \min_{c \in \{\text{R,G,B}\}} I^c(y) / A^c \right], \quad (10)$$

where  $\text{Turbidity}_{\text{level}}(I_k)$  is the turbidity level of input

image  $I_k$ ,  $\eta$  is a parameter to adjust the dehaze level, and  $A^c$  is the ambient light of color channel  $c$ . The higher  $\eta$  is, the higher the dehaze level, which is a variable parameter proportional to the turbidity levels. With  $\eta$  and fast guide filter, the transmission map is improved. The comparison of transmission maps is shown in Fig. 6.

### 3.4 Multiple normalize unsharp masking for detail improvement of underwater images

Details of images are important for the application of computer vision and machine vision [38]. Ancuti et al. [9] proposed the normalized unsharp masking method. The typical formula for unsharp masking defines the sharpened image  $S$  as  $S = I + \beta(I - G * I)$ , where  $I$  is the image to be sharpened.  $G * I$  denotes the Gaussian filtered version of  $I$ , and  $\beta$  is

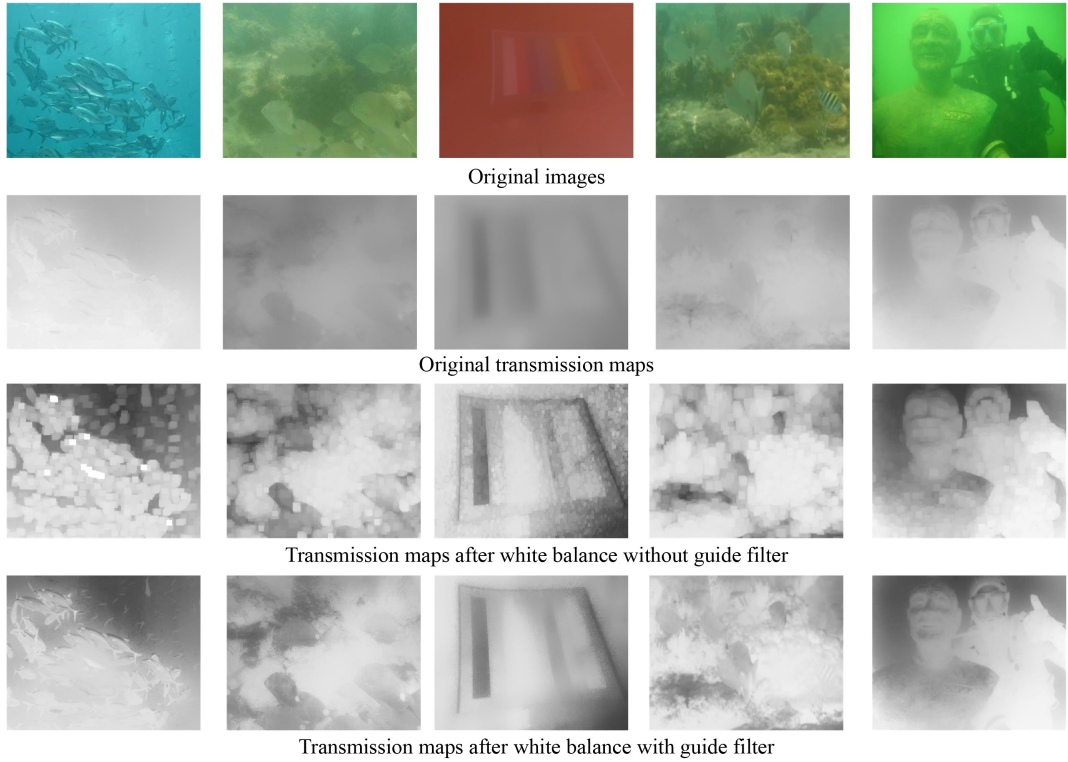


**Fig. 6** Underwater images and transmission maps with different methods.

a parameter. Ancuti believed that the selection of  $\beta$  is not trivial in practice. A small  $\beta$  fails to sharpen  $I$ , but a very large  $\beta$  results in over saturated regions with brighter highlights and darker shadows [9]. Hence, Ancuti proposed the normalized unsharp masking method:

$$S = (I + N\{I - G * I\})/2, \quad (11)$$

where  $N$  is the linear normalization operator.

Enlightened by Ref. [39], our findings reveal that multiple masking is useful for sharpening; thus, normalized unsharp masking is combined with multiple unsharp masking, and our proposed method is called multiple normalize unsharp masking. Gaussian differential filter [40] is used in the method, and three levels of unsharp masking are set by different scales of Gaussian differential filters:

$$\begin{cases} B_0 = I, \\ B_1 = G_1 * I, \\ B_2 = G_2 * I, \\ B_3 = G_3 * I, \end{cases} \quad (12)$$

where  $G_1$ ,  $G_2$ , and  $G_3$  are the standard Gaussian masks with different filter ratio  $\sigma$ ,  $B_0$  is the image without filtering,  $B_1$ ,  $B_2$ , and  $B_3$  are blurred images filtered by  $G_1$ ,  $G_2$ , and  $G_3$ , respectively, and  $*$  is the convolution symbol.

To capture images of different blur degrees,  $\sigma_1 = 1.0$ ,  $\sigma_2 = 2.0$ , and  $\sigma_3 = 4.0$  are set [39].  $B_i$  is processed with linear normalization operator  $N$  to avoid selecting a proper  $\beta$ . Based on the operator, different details maps are obtained, and sharpened image  $I_{\text{sharp}}$  is obtained:

$$I_{\text{sharp}} = I + \sum_{i=0}^2 \frac{2N\{B_{i+1} - B_i\}}{3}. \quad (13)$$

In Ref. [9], the constant of Eq. (13) is 0.5, whereas in our function, the constant is adjusted to 2/3. Our practice tests reveal that the resulting images are slightly darker with the constant 1/2. Thus, the constant is adjusted to 2/3 to improve the luminance of images. The results of sharpening images are shown in Fig. 7. Compared with images without sharpening, the sharpened images have more details that are easier identify.

### 3.5 Image fusion

Compared with enhancement methods alone, image fusion can combine the advantages of several enhancement methods. Different from other image fusion methods [41], in this section, image fusion based on three weight maps, namely, Laplacian weight, saliency weight, and saturation weight, is used. Our fusion method has two input images, and the detection method decides which two images are selected as inputs.

Laplacian maps ( $W_L$ ) work on the luminance channel of input images and assign high values to edges and textures. The ratio of Laplacian mask is 3, and all elements are set as -1, but the center one is 8.

Saliency weight ( $W_S$ ) works on Lab color space. In turbid, dark underwater scenes, objects can lose their prominence and be ignored. To emphasize the main

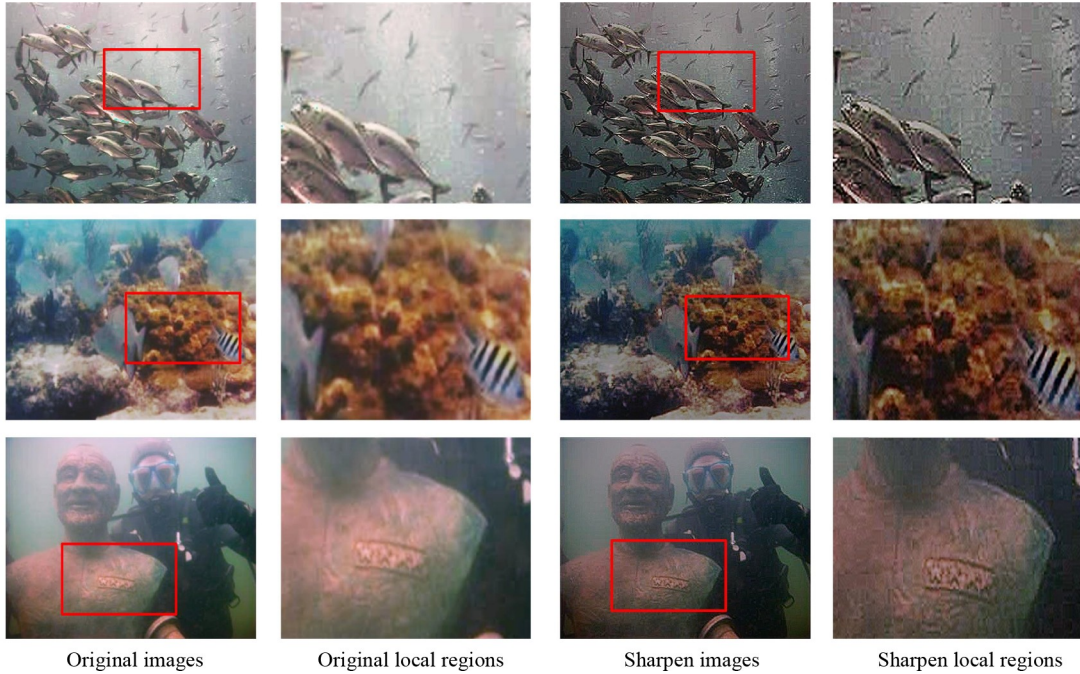


**Fig. 7** Comparative results of original images and sharpened images.

object in underwater images, saliency weight, which sets high values for the main object regions, is adopted. Saliency weight can be obtained as follows:

$$W_S = (L - \bar{L})^2 + (A - \bar{A})^2 + (B - \bar{B})^2, \quad (14)$$

where  $L$ ,  $A$ , and  $B$  are channels of Lab color space, and  $\bar{L}$ ,  $\bar{A}$ , and  $\bar{B}$  are the means of the channels of Lab color space.

Saturation weight ( $W_T$ ) can emphasize the chromatic information of saturated regions, which is lost in underwater images because they are severely dehazed. It can be obtained as follows:

$$W_T = \sqrt{[(R - L)^2 + (G - L)^2 + (B - L)^2] / 3}, \quad (15)$$

where  $R$ ,  $G$ , and  $B$  are the channels of RGB color space, and  $L$  is the luminance channel of Lab color space.

After obtaining the three weight maps, they are normalized into a single weight map:

$$W_k = \left( \sum_{i \in \{L, S, T\}} W_{k,i} + \delta \right) \left/ \left( \sum_{k=1}^K \sum_{i \in \{L, S, T\}} W_{k,i} + K\delta \right) \right., \quad (16)$$

where  $k$  denotes the number of input images,  $K$  is the amount of input images and is equal to 2 because there are two images for fusion in our method, and  $\delta$  denotes a small regularization term that ensures that each input contributes to the output. We set  $\delta = 0.1$  enlightened by Ref. [9]. Two images are selected to show the weight maps, as illustrated in Fig. 8. With normalized weight maps, fusion images  $F(x)$  can typically be obtained by fusing the defined inputs with the weight measures at every location  $x$ :

$$F(x) = \sum_{k=1}^K W_k(x) I_k(x). \quad (17)$$

### 3.6 Algorithm flowchart

To achieve the targets for different environments, the turbidity-adaptive enhancement method is proposed based on the above methods. The flow chart of the algorithm is shown in Fig. 9.

For light turbidity, only white balance is applied to correct color because images captured in this environment are relatively clear. For medium turbidity, white balance, DCP, and sharpening are applied, and the result of white balance and sharpening are set as input images for fusion to obtain the final result. In severe turbidity, the sharpening method is removed because the noise in severe turbid underwater environment is serious, and our target for it is to identify the main object clearly.

---

## 4 Experiment and evaluation

A series of experiments is carried out, and many underwater images are captured and processed using our method. The results are compared with other methods and evaluated by underwater color image quality evaluation metric (UCIQE) [41] and speeded up robust features (SURF) [42].

### 4.1 Experiments

Our experiments have two purposes: Capture several



**Fig. 8** Three weight maps used in image fusion.

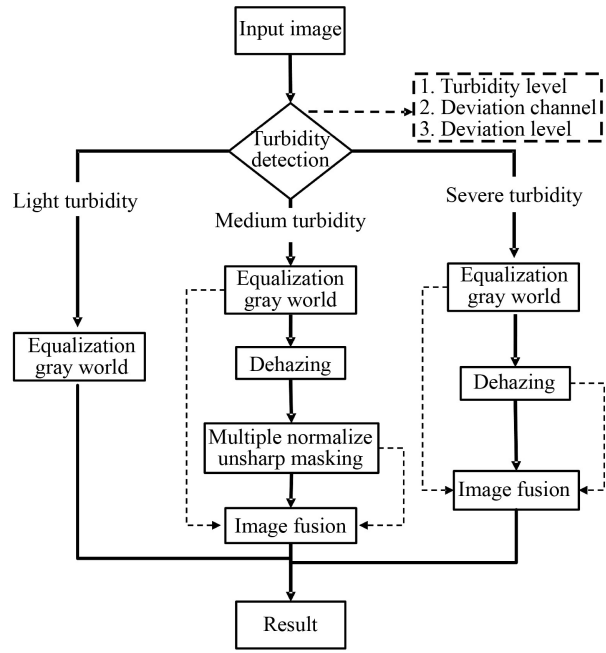


**Fig. 9** Algorithm flowchart of turbidity-adaptive underwater image enhancement method.

moderately turbid underwater images and obtain several special color deviation underwater images. Our research on the papers on underwater image enhancement finds that the underwater environment of those papers is not very turbid, even though several of them focus on turbid underwater. Several of their images are selected for

comparison with the images captured in our experiment, as shown in Fig. 10 [5,33,43,44]. The severe turbid images in our experiments are more turbid than those of other papers. Other than severe turbidity, light and medium turbidity are set in our experiments. To capture different underwater images, dissimilar amounts of varying media are added to the water, and underwater images are captured using GoPro 7 Black produced by DJI technology company. The equipment used is shown in Fig. 11. Blue and red dyes are used to create environments with special color deviation. Four different object distances are set in experiments, namely, 70, 40, 20, and 10 cm.

The different underwater environments in our experiments are shown in Fig. 12, where the number denotes the concentration. More than 300 real underwater images are captured. The devices used are the same as in Fig. 11. With two fixing rods, approximately 1600 underwater images are captured at Songshan Lake.

Two main areas are considered in this experiment, the center of Songshan Lake and the shoal of the lake. Object distances are set as 50, 30, and 10 cm. The depth of shoal is about 40 cm, and the depth of camera at the center of lake is about 20–300 cm. Two special images are used in this experiment, and parts of the images are shown in Fig. 13.

## 4.2 Results

The results of our method are compared with those of other methods [35,45,46]. The results are in two groups: One focuses on images that often appear in other papers,

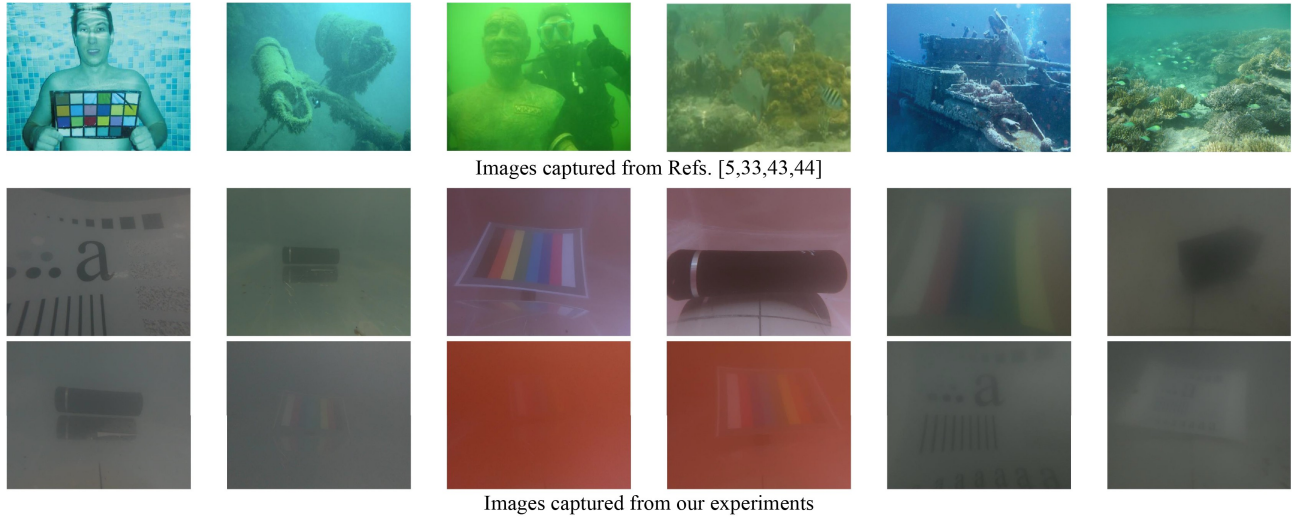


**Fig. 10** Image comparison of other papers and our experiment. The images in the first row are cited from Refs. [5,33,43,44] with permission from Elsevier.

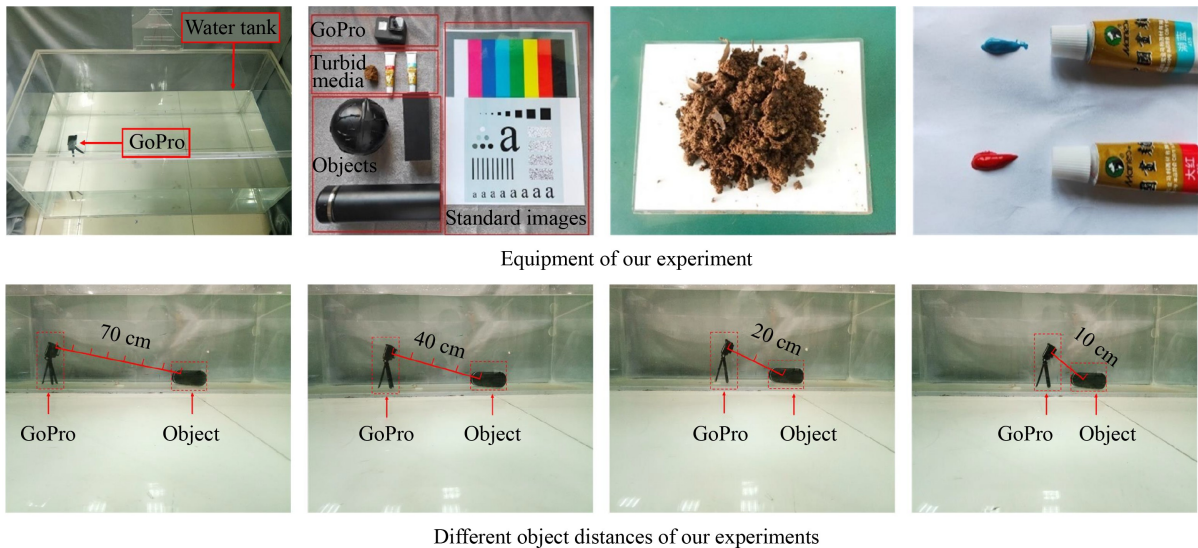


**Fig. 11** Equipment and parameter setting of our experiments.

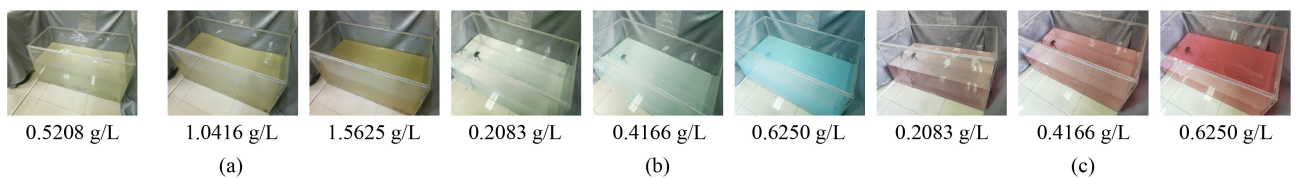


**Fig. 12** Different turbid waters in our experiments: (a) soil waters changing from light to severe, (b) blue waters changing from light to severe, and (c) red waters changing from light to severe.

and another focuses on the images of our experiments. The two groups of results are shown in Figs. 14 and 15 [35,45,46]. Moreover, real underwater images are captured and processed by our methods, and the results are shown in Fig. 16 [35,45,46]. The resulting images of the different stages of our method are shown in Figs. A1–A3 in the Appendix.

#### 4.3 Discussion

UCIQE, SSIM, and SURF are used to evaluate the result of our method. UCIQE is calculated as follows:

$$E_{UCIQE} = c_1 C_{var} + c_2 L_{con} + c_3 S_{aver}, \quad (18)$$

where  $c_1$ ,  $c_2$ , and  $c_3$  are the weight coefficients set as

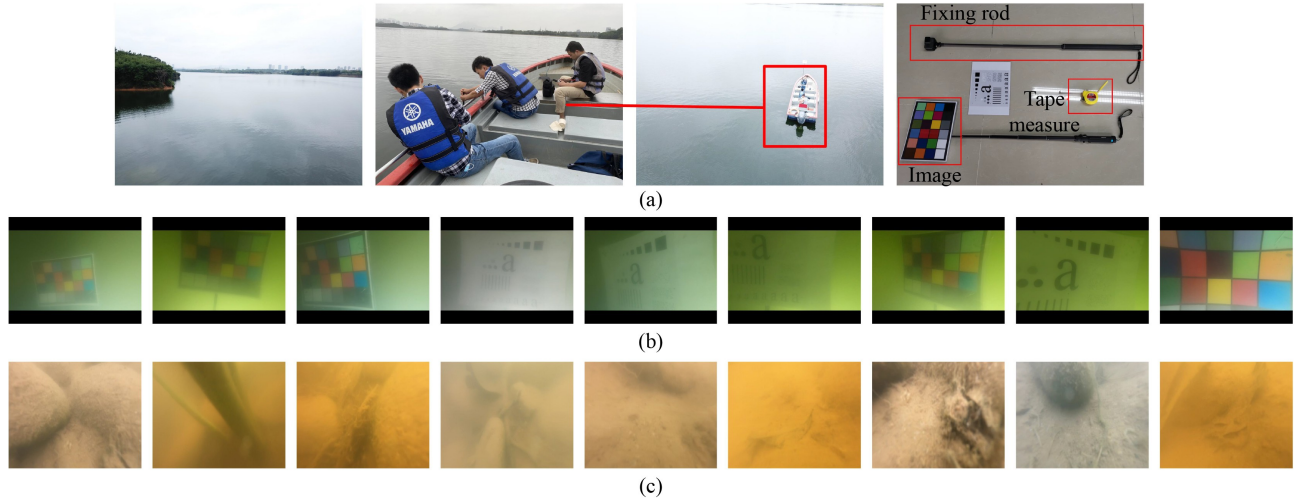


**Fig. 13** Images captured at Songshan Lake. (a) Platform and devices, (b) images captured with different objects at Songshan Lake, and (c) images of the shoal of Songshan Lake.

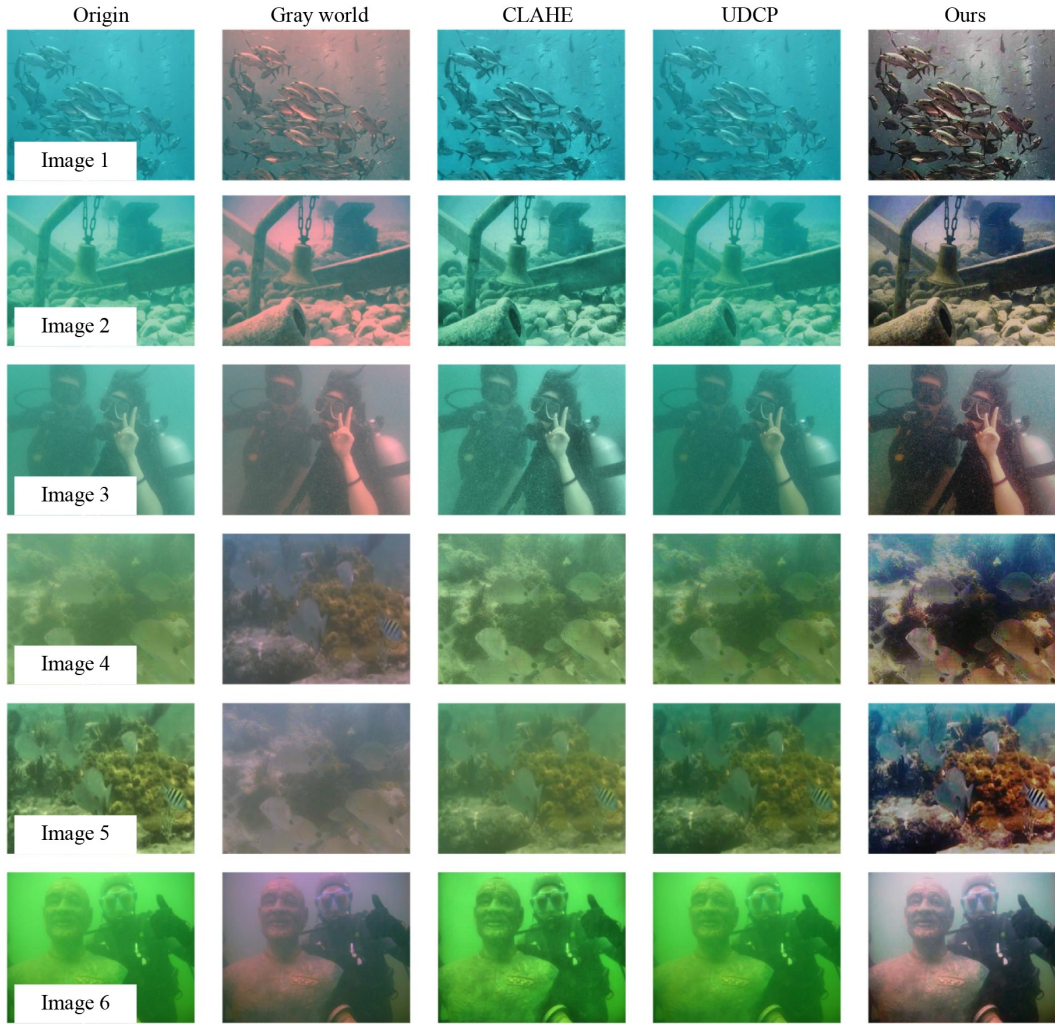


**Fig. 14** Comparison of different enhancement methods of other papers: gray world [46], contrast limited adaptive histogram equalization (CLAHE) [45], and underwater dark channel prior (UDCP) [35].

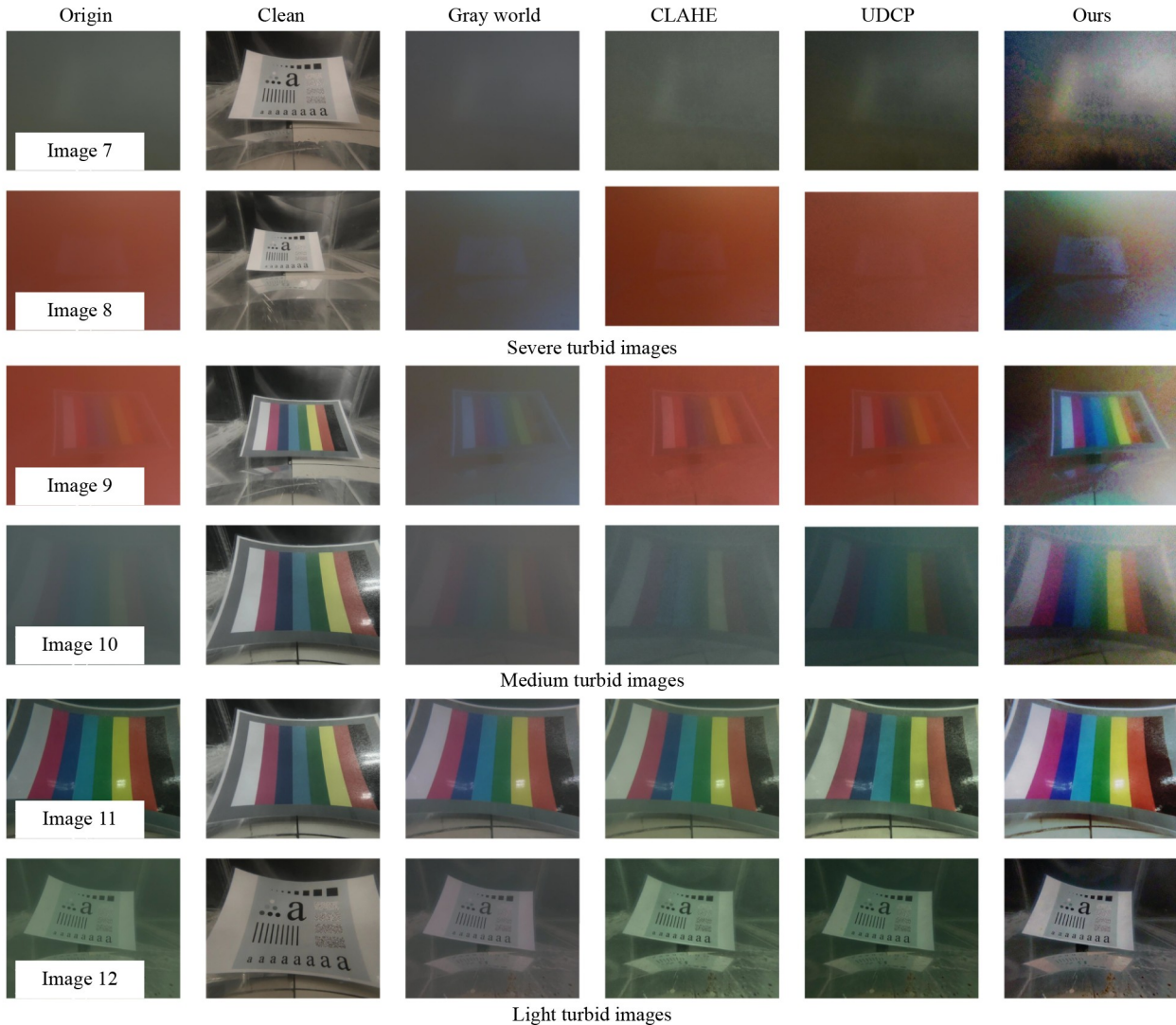


**Fig. 15** Comparison of different enhancement methods in our experiments: gray world [46], CLAHE [45], and UDCP [35].

$c_1 = 0.4680$ ,  $c_2 = 0.2745$ , and  $c_3 = 0.2576$  [47],  $C_{\text{var}}$  is the standard deviation of chroma,  $L_{\text{con}}$  is the contrast of luminance, and  $S_{\text{aver}}$  is the average of saturation. The UCIQE values of the images in Figs. 14–16 [35,45,46] are shown in Tables A1 and A2 in the Appendix. UCIQE values are improved with different image enhancement methods, but the improvement of the method proposed in this paper is the highest. SURF is used to match feature points of images. The original images are rotated by 45° counter clockwise to set them as the patch targets of the original images.

Figure 17 shows UCIQE and SSIM of all our images including images of our experiments, images of other papers, and images captured in a real lake: 1053 real underwater images, 242 experiment underwater images, and 18 images of other papers. SSIM is applied only for experiment images because original images captured in clean water of images of real lake and other papers cannot be obtained.

The SURF results in Fig. 18 show that the match point pairs of the resulting images increase by more than 50% than the original images.

In SSIM metric, images captured in clean water of our experiments are selected as reference for other images. Compared with other methods, the metric values of our method are higher. A total of 1313 images are processed by our method, including images of other papers, experiment images, and real underwater images. Most resulting images are better than the original images. The UCIQE of the result images is higher than that of the original images, and the result of SURF is better.

## 5 Conclusions

In this paper, an enhancement algorithm called a turbidity-adaptive underwater image enhancement method using image fusion, which can enhance underwater images with different routes based on

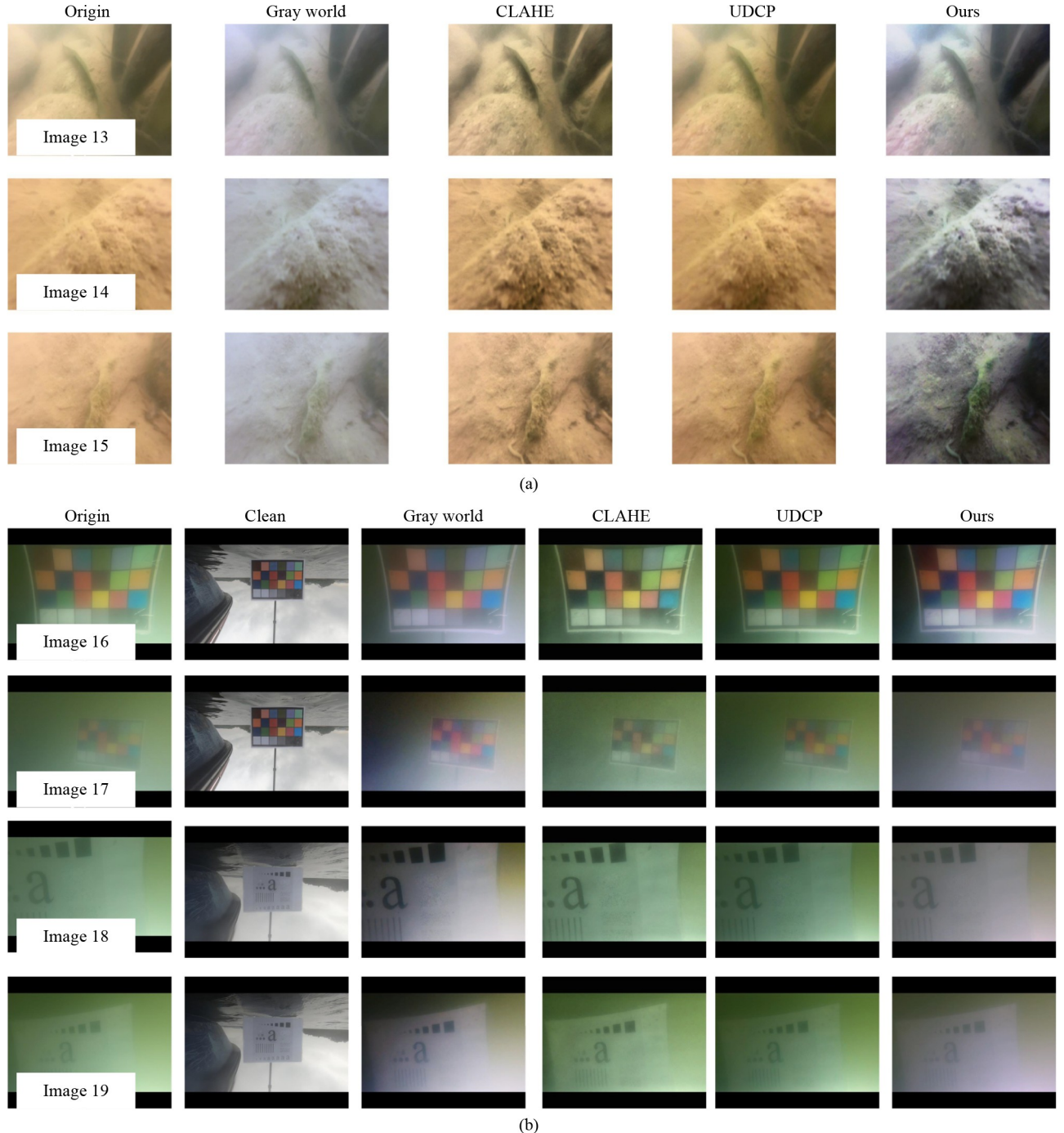


**Fig. 16** Comparison of different enhancement methods of real underwater images, namely, gray world [46], CLAHE [45], and UDCP [35]: (a) results of the shoal of Songshan Lake and (b) results of Songshan Lake.

turbidity levels, is proposed. This method is used to process different underwater images from experiments and other papers to verify that it works well on different turbid underwater environments. This method is also compared with other papers, and the results are evaluated using UCIQE and SURF.

The results show that the proposed method can adapt to different turbidity conditions and improve the quality of

images effectively in severe turbid underwater images. However, for deep severe turbid underwater environment, where artificial light is imported, image enhancement entails more difficulties, and our algorithm has not been used to deal with this special case. Future work will address the special harsh underwater environment. For most underwater images, color deviation, image textures, and image quality are improved after processing by the

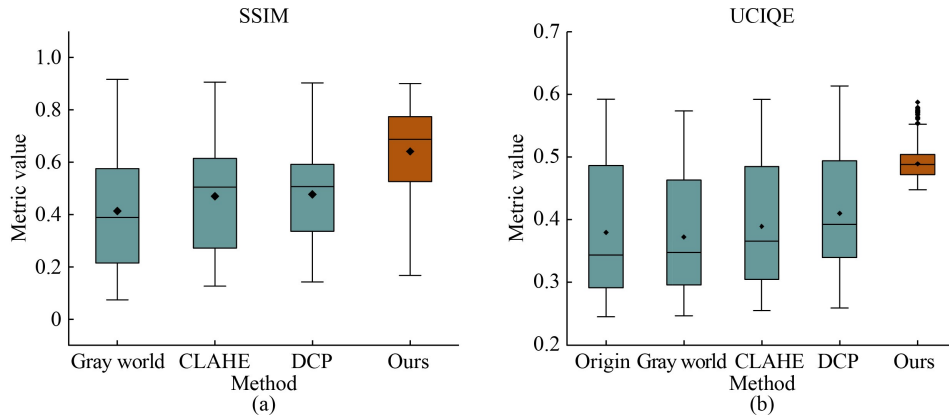


**Fig. 17** (a) SSIM and (b) UCIQE results of different methods. UCIQE is obtained from all underwater images including images of our experiment, images of other papers, and real underwater images captured from a lake. SSIM is taken from all underwater images of our experiments. The original images of clean water are selected as reference of other processed images.

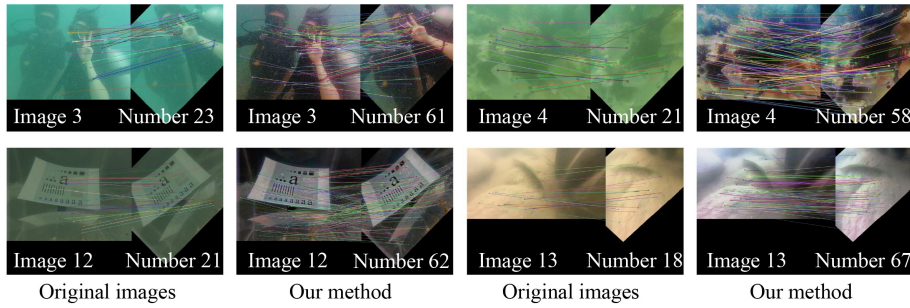


**Fig. 18** SURF results of original images and our method.

proposed method, which is helpful for the work of underwater robotics.

## Nomenclature

$A$	Ambient light	$Deviation_c$	Deviation of color channel $c$
$A^c$	Ambient light of color channel $c$	$Deviation_{level}$	Color deviation level
$B$	Blurred image	$Deviation_{max}$	Maximum deviation of image
$B_i$ ( $i = 0, 1, 2, 3$ )	$B_0$ is the image without filtering. $B_1$ , $B_2$ and $B_3$ are blurred images filtered by $G_1$ , $G_2$ , and $G_3$ , respectively	$E_{UCIQE}$	Value of UCIQE of image
$B_\infty(x)^c$	Value of infinite pixel $x$ of color channels $c$ of ambient light image	$F(x)$	Fusion image
$c$	Color channel (R, G, B) of image	$G$	Gaussian differential filter
$c_1, c_2, c_3$	$c_1$ , $c_2$ , and $c_3$ are the weight coefficients set as $c_1 = 0.4680$ , $c_2 = 0.2745$ , and $c_3 = 0.2576$	$G_i$ ( $i = 1, 2, 3$ )	Gaussian differential filter with different filter ratio
$C_{i1}, C_{i2}$	Two other channels in addition to attenuation channel	$I$	Image to be sharpened
$\overline{C_{i1}}, \overline{C_{i2}}$	Average of $C_{i1}$ and $C_{i2}$ , respectively	$I(x)$	Pixel value at $x$ of image $I$
$\overline{C}_j$	Mean of attenuation channel	$I^c(x)$	Pixel value at $x$ of color channel $c$ of degraded image
$C_{jc}$	Compensation channel	$I_k(x)$	Number $k$ input image
$C_{var}$	Standard deviation of chroma	$I_{sharp}$	Sharpened image
$d(x)$	Object distance of pixel $x$	$I_{var}$	Variance of channels
		$J$	Undegraded image
		$J^c(x)$	Pixel value at $x$ of color channel $c$ of original image
		$J_{dark}$	Dark channel images
		$K$	Amount of input images
		$L, A, B$	Channels of Lab color space
		$L_1, L_2$	Thresholds for color deviation level detecting, and they are set as 40 and 60, respectively
		$\overline{L}, \overline{A}, \overline{B}$	Means of channels of Lab color space

$L_{\text{con}}$	Contrast of luminance
$m$	Constant parameter for compensation, it is set as 0.18
$\text{Mean}_c$	Mean of color channel $c$
$\text{Mean}_{\text{sum}}$	Mean of all color channels of image
$n$	Constant parameter for compensation, it is set as 0.15
$N$	Linear normalization operator, also named histogram stretching in the literature
$S$	Sharpened image in normalized unsharp masking method
$S_{\text{aver}}$	Average of saturation
$T(x)$	Pixel value at $x$ of transmission map
$T_1, T_2$	Variance thresholds for turbidity level detecting, and they are set as 9 and 28, respectively
$T^c(x)$	Pixel value at $x$ of color channel $c$ of transmission map
$\text{Turbidity}_{\text{level}}$	Turbidity level of image
$w$	Compensation level
$W_k$	Normalized weight map
$W_L$	Laplacian weight map
$W_S$	Saliency weight map
$W_T$	Saturation weight map
$x$	Localization of pixel
$y$	Pixel localization of region $\Omega(x)$
$\alpha$	Attenuation coefficient of water
$\beta$	Special parament in normalized unsharp masking method
$\eta$	Parameter to adjust the dehaze level
$\delta$	A small regularization term that ensures that each input contributes to the output, and it is set as 0.1
$\Omega(x)$	Local region centered at pixel $x$
$\sigma$	Filter ratio

## Appendix

**Table A1** Underwater image evaluation based on UCIQE

Image	Underwater image evaluation				
	Origin	Gray world	CLAHE	UDCP	Our method
1	0.29482	0.39397	0.34491	0.30368	0.49016
2	0.34675	0.39382	0.38193	0.36540	0.50846
3	0.33249	0.34176	0.35667	0.39435	0.52372
4	0.36472	0.37469	0.40091	0.41527	0.53806
5	0.33711	0.43044	0.38948	0.35630	0.51864
6	0.39073	0.41309	0.41042	0.41415	0.51215
7	0.30806	0.30848	0.31754	0.33841	0.51689
8	0.29159	0.29569	0.29350	0.34770	0.48641
9	0.30773	0.32783	0.31055	0.33060	0.48963
10	0.30766	0.30950	0.31975	0.37578	0.51486
11	0.33487	0.33830	0.36050	0.39308	0.46614
12	0.29352	0.29745	0.29799	0.35100	0.50293
13	0.28471	0.28601	0.29181	0.34124	0.47248
14	0.34364	0.36475	0.36003	0.37045	0.45168
15	0.31619	0.33560	0.3320	0.34455	0.46578
16	0.53360	0.51917	0.53510	0.54501	0.55259
17	0.50480	0.48477	0.50146	0.51459	0.52190
18	0.47984	0.43658	0.47940	0.47915	0.49416
19	0.49808	0.47624	0.49343	0.50811	0.50991

**Table A2** Average of UCIQE of Table A1

Method	Image average evaluation	Image amplification/%
Origin	0.361627	100.0
Gray world	0.375165	103.7
CLAHE	0.377757	104.4
UDCP	0.394148	108.9
Our method	0.501924	138.7

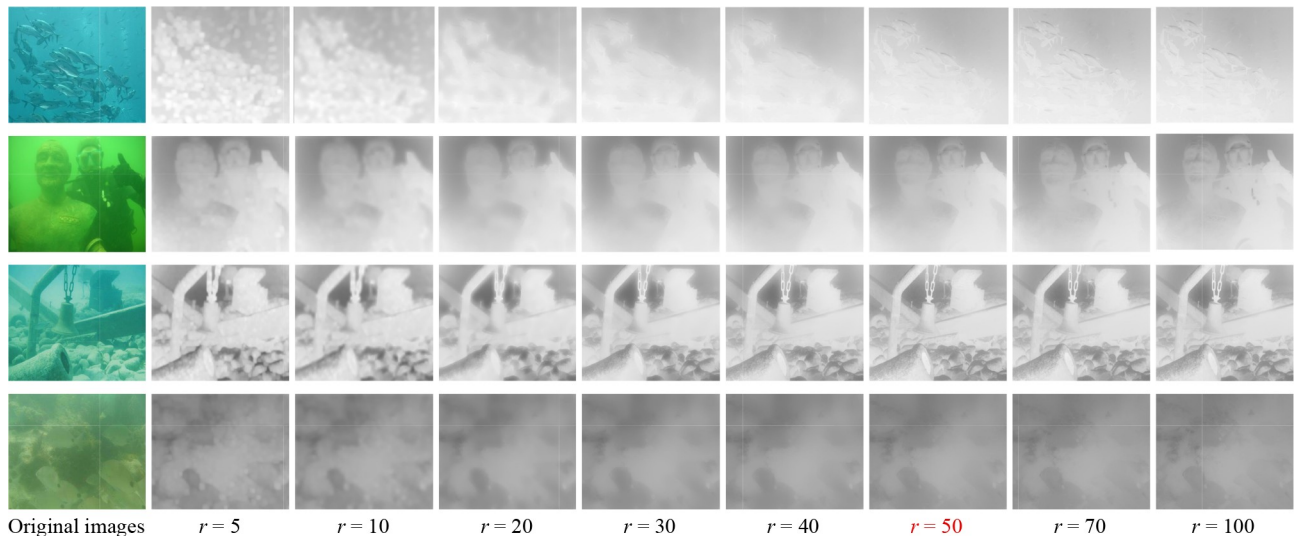


**Fig. A1** Transmission maps of guide filter based on different ratios.

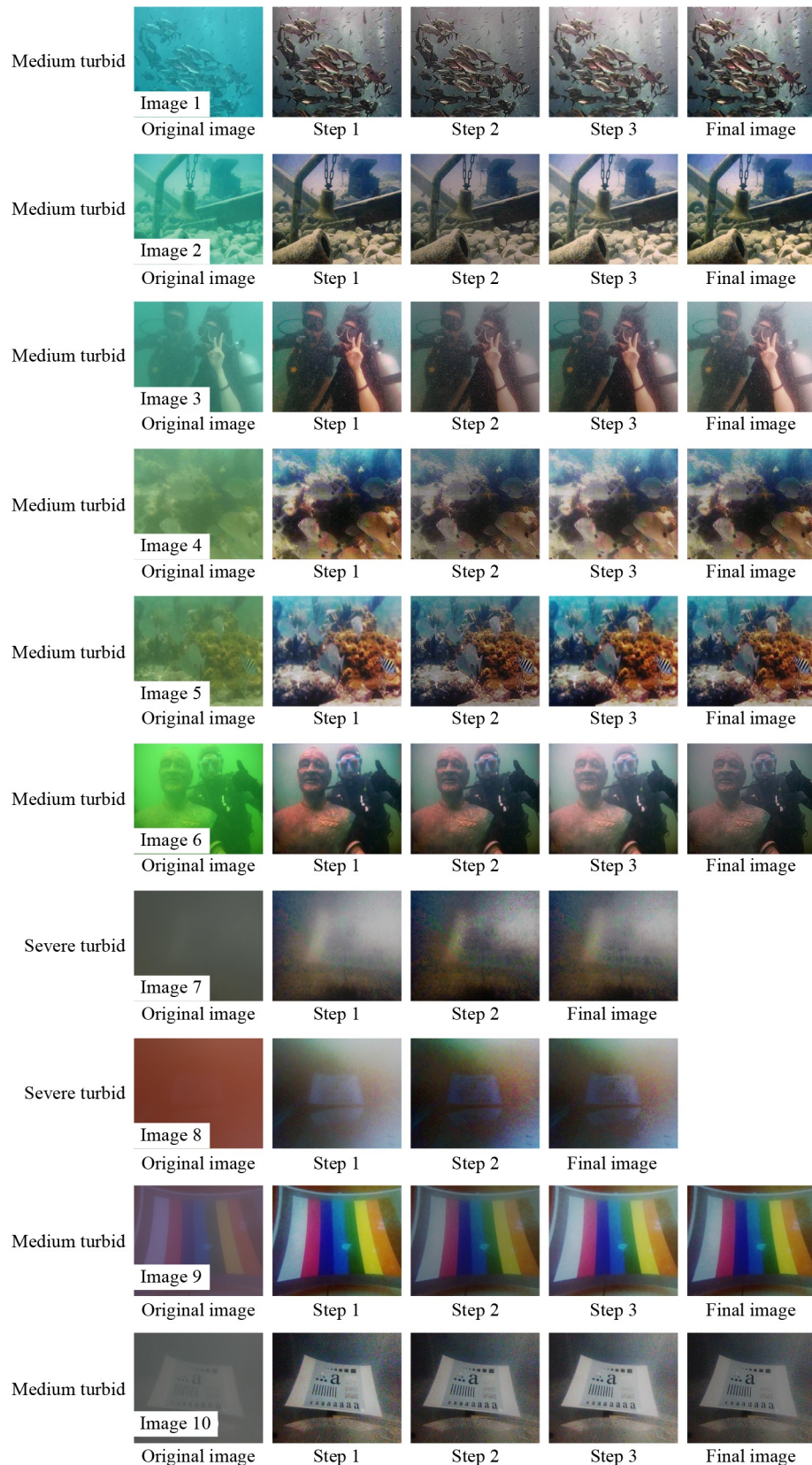


**Fig. A2** Intermediate results of images 1–10.

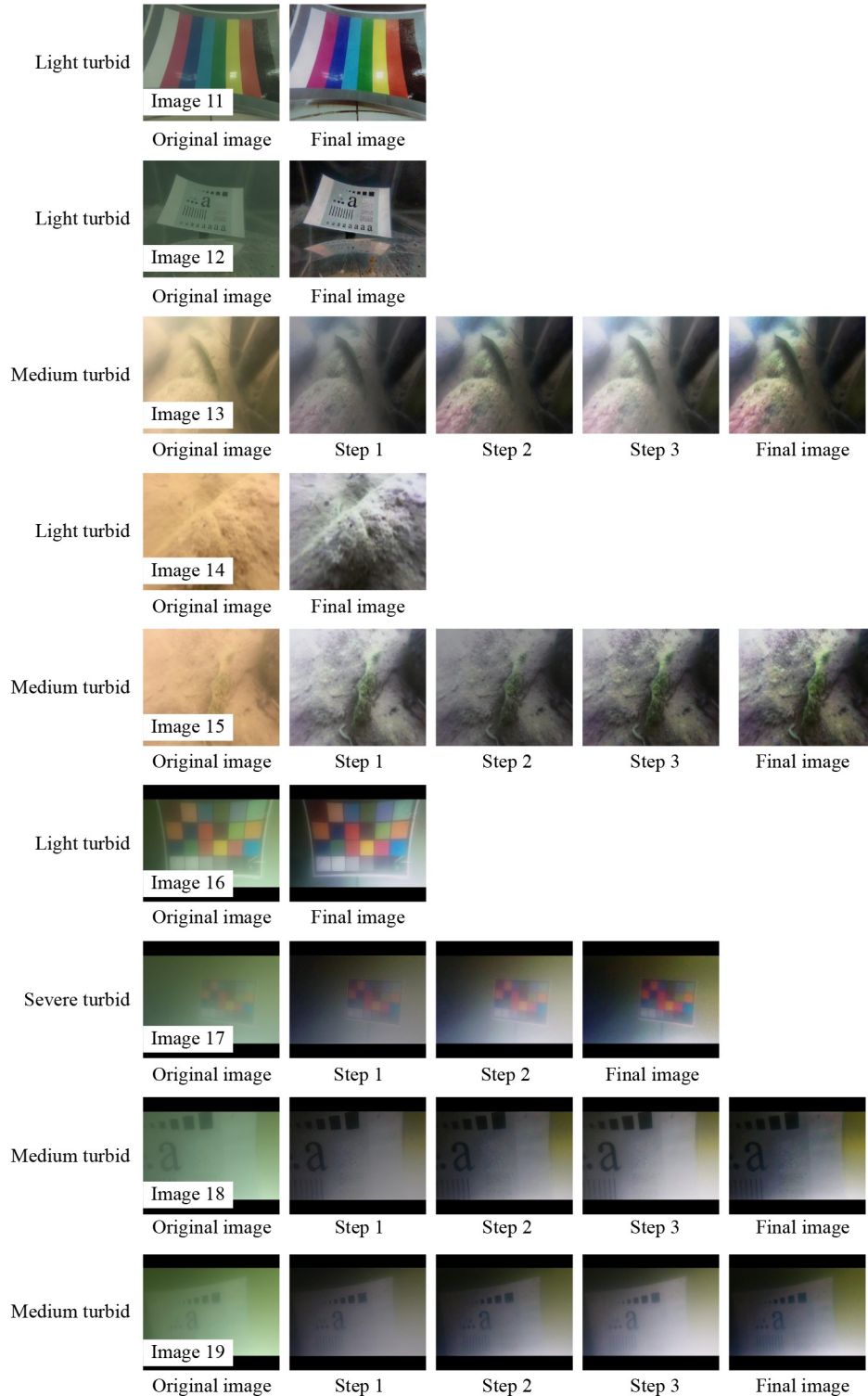


**Fig. A3** Intermediate results of images 11–19.

**Acknowledgements** This work was supported by the Guangdong Innovative and Entrepreneurial Research Team Program, China (Grant No. 2019ZT08Z780), in part by the Dongguan Introduction Program of Leading Innovative and Entrepreneurial Talents, China, in part by the National Key R&D Program of China (Grant No. 2017YFC0821200), in part by the

Guangdong Basic and Applied Basic Research Foundation, China (Grant No. 2021A1515011717), and in part by the Space Trusted Computing and Electronic Information Technology Laboratory of BICE, China (Grant No. OBCandETL-2020-06).

## References

1. Boudhane M, Nsiri B. Underwater image processing method for fish localization and detection in submarine environment. *Journal of Visual Communication and Image Representation*, 2016, 39: 226–238
2. Lin Y H, Yu C M, Wu C Y. Towards the design and implementation of an image-based navigation system of an autonomous underwater vehicle combining a color recognition technique and a fuzzy logic controller. *Sensors*, 2021, 21(12): 4053
3. Liu J G, Wang Y C, Li B, Ma S G. Current research, key performances and future development of search and rescue robots. *Frontiers of Mechanical Engineering*, 2007, 2(4): 404–416
4. Li T C, Wang J L, Yao K N. Visibility enhancement of underwater images based on active polarized illumination and average filtering technology. *Alexandria Engineering Journal*, 2022, 61(1): 701–708
5. Zhuang P X, Li C Y, Wu J M. Bayesian retinex underwater image enhancement. *Engineering Applications of Artificial Intelligence*, 2021, 101: 104171
6. Liang Z, Wang Y F, Ding X Y, Mi Z T, Fu X P. Single underwater image enhancement by attenuation map guided color correction and detail preserved dehazing. *Neurocomputing*, 2021, 425: 160–172
7. Li C Y, Anwar S, Hou J H, Cong R M, Guo C L, Ren W Q. Underwater image enhancement via medium transmission-guided multi-color space embedding. *IEEE Transactions on Image Processing*, 2021, 30: 4985–5000
8. Ancuti C, Ancuti C O, Haber T, Bekaert P. Enhancing underwater images and videos by fusion. In: Proceedings of 2012 IEEE CVPR Conference. 2012, 81–88
9. Ancuti C O, Ancuti C, De Vleeschouwer C, Bekaert P. Color balance and fusion for underwater image enhancement. *IEEE Transactions on Image Processing*, 2018, 27(1): 379–393
10. Wang Y, Zhang J, Cao Y, Wang Z F. A deep CNN method for underwater image enhancement. In: Proceedings of 2017 IEEE International Conference on Image Processing (ICIP). IEEE, 2017, 1382–1386
11. Guo Y C, Li H Y, Zhuang P X. Underwater image enhancement using a multiscale dense generative adversarial network. *IEEE Journal of Oceanic Engineering*, 2020, 45(3): 862–870
12. Liu R S, Fan X, Zhu M, Hou M J, Luo Z X. Real-world underwater enhancement: challenges, benchmarks, and solutions under natural light. *IEEE Transactions on Circuits and Systems for Video Technology*, 2020, 30(12): 4861–4875
13. Fu X Y, Cao X Y. Underwater image enhancement with global-local networks and compressed-histogram equalization. *Signal Processing: Image Communication*, 2020, 86: 115892
14. Yang M, Hu K, Du Y X, Wei Z Q, Sheng Z B, Hu J T. Underwater image enhancement based on conditional generative adversarial network. *Signal Processing: Image Communication*, 2020, 81: 115723
15. Jiang Q, Zhang Y F, Bao F X, Zhao X Y, Zhang C M, Liu P D. Two-step domain adaptation for underwater image enhancement. *Pattern Recognition*, 2022, 122: 108324
16. Li C Y, Guo C L, Ren W Q, Cong R M, Hou J H, Kwong S, Tao D C. An underwater image enhancement benchmark dataset and beyond. *IEEE Transactions on Image Processing*, 2020, 29: 4376–4389
17. Liu Y Q, Chen Y Y, Fang X M. A review of turbidity detection based on computer vision. *IEEE Access: Practical Innovations, Open Solutions*, 2018, 6: 60586–60604
18. Chen S S, Han L S, Chen X Z, Li D, Sun L, Li Y. Estimating wide range total suspended solids concentrations from MODIS 250-m imageries: an improved method. *ISPRS Journal of Photogrammetry and Remote Sensing*, 2015, 99: 58–69
19. Zhang X H. Water quality turbidity detection based on image recognition system design and implementation. In: Proceedings of 2016 the First International Conference on Real Time Intelligent Systems. 2018, 613: 63–70
20. O’Byrne M, Schoefs F, Pakrashi V, Ghosh B. An underwater lighting and turbidity image repository for analysing the performance of image-based non-destructive techniques. *Structure and Infrastructure Engineering*, 2018, 14(1): 104–123
21. Xie K, Pan W, Xu S X. An underwater image enhancement algorithm for environment recognition and robot navigation. *Robotics*, 2018, 7(1): 14
22. Hu H F, Zhang Y B, Li X B, Lin Y, Cheng Z Z, Liu T G. Polarimetric underwater image recovery via deep learning. *Optics and Lasers in Engineering*, 2020, 133: 106152
23. Wang Y B, Cao J, Rizvi S, Hao Q, Fang Y M. Underwater image restoration based on adaptive color compensation and dual transmission estimation. *IEEE Access: Practical Innovations, Open Solutions*, 2020, 8: 207834–207843
24. Zhang W H, Li G, Ying Z Q. A new underwater image enhancing method via color correction and illumination adjustment. *2017 IEEE Visual Communications and Image Processing*, 2017, 1–4
25. Jaffe J S. Computer modeling and the design of optimal underwater imaging systems. *IEEE Journal of Oceanic Engineering*, 1990, 15(2): 101–111
26. Amer K O, Elbouz M, Alfalou A, Brosseau C, Hajjami J. Enhancing underwater optical imaging by using a low-pass polarization filter. *Optics Express*, 2019, 27(2): 621–643
27. Li Y J, Lu H M, Li K C, Kim H, Serikawa S. Non-uniform de-scattering and de-blurring of underwater images. *Mobile Networks and Applications*, 2018, 23(2): 352–362
28. Peng Y T, Cosman P C. Underwater image restoration based on image blurriness and light absorption. *IEEE Transactions on Image Processing*, 2017, 26(4): 1579–1594
29. Huang J, Liu G X. Multi-color space threshold segmentation and self-learning  $k$ -NN algorithm for surge test EUT status identification. *Frontiers of Mechanical Engineering*, 2016, 11(3): 311–315
30. Zhu D Q, Liu Z Q, Zhang Y M. Underwater image enhancement based on colour correction and fusion. *IET Image Processing*, 2021, 15(11): 2591–2603
31. Yang X, Li H, Chen R. Underwater image enhancement with image colorfulness measure. *Signal Processing: Image Communication*, 2021, 95: 116225
32. Wang Y Q, Yu X N, An D, Wei Y G. Underwater image enhancement and marine snow removal for fishery based on

- integrated dual-channel neural network. *Computers and Electronics in Agriculture*, 2021, 186: 106182
- 33. Galdran A, Pardo D, Picón A, Alvarez-Gila A. Automatic red-channel underwater image restoration. *Journal of Visual Communication and Image Representation*, 2015, 26: 132–145
  - 34. He K M, Sun J, Tang X O. Single image haze removal using dark channel prior. *IEEE Transactions on Pattern Analysis and Machine Intelligence*, 2011, 33(12): 2341–2353
  - 35. Yu H F, Li X B, Lou Q, Lei C B, Liu Z X. Underwater image enhancement based on DCP and depth transmission map. *Multimedia Tools and Applications*, 2020, 79(27–28): 20373–20390
  - 36. Zhang M H, Peng J H. Underwater image restoration based on a new underwater image formation model. *IEEE Access: Practical Innovations, Open Solutions*, 2018, 6: 58634–58644
  - 37. He K M, Sun J, Tang X O. Guided image filtering. *IEEE Transactions on Pattern Analysis and Machine Intelligence*, 2013, 35(6): 1397–1409
  - 38. Wei L S, Jiao Z X. Research and application of visual location technology for solder paste printing based on machine vision. *Frontiers of Mechanical Engineering*, 2009, 4(2): 184–191
  - 39. Lin S, Chi K C, Li W T, Tang Y D. Underwater optical image enhancement based on dominant feature image fusion. *Acta Photonica Sinica*, 2020, 49(3): 310003
  - 40. Kim Y, Koh Y J, Lee C, Kim S, Kim C S. Dark image enhancement based on pairwise target contrast and multi-scale detail boosting. In: *Proceedings of 2015 IEEE International Conference on Image Processing*. 2015, 1404–1408
  - 41. Shen D H, Zareapoor M, Yang J. Multimodal image fusion based on point-wise mutual information. *Image and Vision Computing*, 2021, 105: 104047
  - 42. Bay H, Tuytelaars T, Goo L V. Surf: speeded up robust features. In: *Proceedings of 2006 the 9th European Conference on Computer Vision*. 2006, 3951, 404–417
  - 43. Huang Y F, Liu M Y, Yuan F. Color correction and restoration based on multi-scale recursive network for underwater optical image. *Signal Processing: Image Communication*, 2021, 93: 116174
  - 44. Mi Z T, Li Y Y, Wang Y F, Fu X P. Multi-purpose oriented real-world underwater image enhancement. *IEEE Access: Practical Innovations, Open Solutions*, 2020, 8: 112957–112968
  - 45. Chang Y K, Jung C, Ke P, Song H, Hwang J. Automatic contrast-limited adaptive histogram equalization with dual gamma correction. *IEEE Access: Practical Innovations, Open Solutions*, 2018, 6: 11782–11792
  - 46. Buchsbaum G. A spatial processor model for object colour perception. *Journal of the Franklin Institute*, 1980, 310(1): 1–26
  - 47. Yang M, Sowmya A. An underwater color image quality evaluation metric. *IEEE Transactions on Image Processing*, 2015, 24(12): 6062–6071